

# Nonlinear parametric excitation of an evolutionary dynamical system

Rocio E Ruelas<sup>1</sup>, David G Rand<sup>2</sup> and Richard H Rand<sup>3,4</sup>

Proc IMechE Part C:  
J Mechanical Engineering Science  
0(0) 1–9  
© IMechE 2011  
Reprints and permissions:  
sagepub.co.uk/journalsPermissions.nav  
DOI: 10.1177/0954406211432066  
pic.sagepub.com



## Abstract

Nonlinear parametric excitation refers to the nonlinear analysis of a system of ordinary differential equations with periodic coefficients. In contrast to linear parametric excitation, which offers determinations of the stability of equilibria, nonlinear parametric excitation has as its goal the structure of the phase space, as given by a portrait of the Poincaré map. In this article, perturbation methods and numerical integration are applied to the replicator equation with periodic coefficients, being a model from evolutionary game theory where evolutionary dynamics are added to classical game theory using differential equations. In particular, we study evolution in the Rock–Paper–Scissors game, which has biological and social applications. Here, periodic coefficients could represent seasonal variation.

## Keywords

Evolutionary dynamics, parametric excitation, multiple scale perturbation method

Date received: 3 October 2011; accepted: 28 November 2011

## Introduction

The field of evolutionary dynamics describes the process of Darwinian evolution ('survival of the fittest') mathematically.<sup>1</sup> To do so, game theory (representing the interaction between different organisms) is combined with differential equations (representing the gradual changes associated with Newtonian physics). Game theory formalizes multi-player interactions by describing how much each player gains or loses as a function of which strategy they choose to play, as well as the strategy chosen by the other players. In this article, we will focus on the 'Rock–Paper–Scissors' (RPS) game. In RPS, players interact in pairs, and one of three strategies is available for each player: rock (R), paper (P) or scissors (S). The payoff structure is such that rock beats scissors, scissors beats paper, and paper beats rock, with the winner earning +1 and the loser earning –1. The resulting payoff matrix is thus given by

$$\begin{matrix} & \begin{matrix} R & P & S \end{matrix} \\ \begin{matrix} R \\ P \\ S \end{matrix} & \begin{pmatrix} 0 & -1 & +1 \\ +1 & 0 & -1 \\ -1 & +1 & 0 \end{pmatrix} \end{matrix} \quad (1)$$

These payoffs represent reproductive success in the context of evolutionary game theory. When modeling genetic evolution, reproductive success is measured in

number of offspring, but evolutionary game theoretic models can also represent 'cultural evolution' or social learning among humans. Here, people preferentially imitate the strategies of successful others, and reproductive success is measured in likelihood of being imitated. Such social learning models can quantitatively reproduce behavior from human behavioral experiments.<sup>2,3</sup>

Survival of the fittest dictates that strategies which earn higher payoffs become more common over time. To add this dynamical element to game theory, the payoff matrix is combined with differential equations. One common approach is given by the 'replicator equation'.<sup>1,4,12</sup> This is a differential equation whose coefficients are taken from an associated payoff matrix. Let  $A_{ij}$  be the payoff of strategy  $i$  playing against strategy  $j$  in a model involving a well-mixed infinitely large

<sup>1</sup>Center for Applied Mathematics, Cornell University, USA

<sup>2</sup>Program for Evolutionary Dynamics, Harvard University, USA

<sup>3</sup>Department of Mechanical and Aerospace Engineering, Cornell University, USA

<sup>4</sup>Department of Mathematics, Cornell University, USA

## Corresponding author:

RH Rand, Department of Mathematics, Cornell University, Ithaca, NY 14853, USA  
Email: rrand@cornell.edu

population of players. We define  $x_i$  as the fraction of players in the population using strategy  $i$ . Assuming there are  $N$  possible strategies, we have the constraint

$$\sum_{i=1}^N x_i = 1 \quad (2)$$

The 'fitness' of an individual playing strategy  $i$  is given by

$$f_i = \sum_{j=1}^N A_{ij} x_j \quad (3)$$

and the replicator equation stipulates that

$$\dot{x}_i = x_i(f_i - \Phi) \quad (4)$$

where  $\Phi$  is chosen, so that the constraint (2) is satisfied. Differentiating (2) and using (4), we must have

$$\sum_{i=1}^N x_i(f_i - \Phi) = 0 \quad (5)$$

Solving for  $\Phi$ , we have

$$\Phi = \sum_{j=1}^N x_j f_j \quad (6)$$

where we have used equation (2).

Equation (4) can then be used to study the evolutionary dynamics of a particular game. In this article, we focus on RPS, which serves a model for many applications in both biology and social science. For example, an RPS dynamic is exhibited in mating behavior of the side-blotched lizard *Uta stansburiana*.<sup>5</sup> Males that keep large territories outcompete males that keep small territories; males that sneak into the territories of others and mate with unprotected females outcompete males with large territories (which are hard to patrol); and males with small territories outcompete sneaker males (because they can effectively defend their smaller territories). Similarly, the bacteria *Escherichia coli*<sup>6</sup> can also have an RPS dynamic. A strain of the bacteria that produces a toxin and an antidote outcompetes the regular ('wild-type') strain; a strain that only produces the antidote outcompetes a strain that makes both the toxin and the antidote (because the toxin is costly to produce, but ineffective if both produce the antidote); and the wild-type strain outcompetes the strain which produces only antidote (because the antidote is also costly to produce, and useless in the absence of toxin).

RPS dynamics also occur in human interactions. For example, consider voluntary cooperative relationships where people can choose whether to work together on a common project.<sup>7,8</sup> There are three different strategies in such an interaction: cooperators choose to participate in the project and do their fair share of work; defectors also choose to participate in the project, but take advantage of the work of others; and loners choose to work on

their own. Defectors exploit cooperators by avoiding the time, effort and cost of contributing while still benefiting from contributions of the cooperators. Thus, a population of cooperators can be overcome by defectors. But in a population of defectors, no one contributes and group projects always fail. Therefore, it is better to work on your own, and loners can overcome a population of defectors. In a population of loners, however, no defectors exist to exploit cooperators. Therefore, it would be best to work together as a group, and cooperators can dominate a population of loners.

In this article, we add periodic variation in payoffs to the RPS game. These periodic effects could represent, for example, fitness changes caused by seasonal fluctuations in the weather, or earning changes caused by seasonal variation in consumer spending. It has been previously shown that when oscillations in payoff are sufficiently fast, periodic coefficients in a two-player game can be reduced to constant coefficients in a multi-player game, leading to stable co-existence.<sup>9</sup>

This article extends a previous paper by our research group<sup>10</sup> by featuring the effect of nonlinear terms in the replicator equations; Rand et al.<sup>10</sup> considered only linear terms.

## Model

We are interested in the effect of replacing the constant coefficients in the RPS payoff matrix (1) by periodic coefficients, for example of the form

$$\begin{array}{c} R \\ P \\ S \end{array} \begin{array}{ccc} R & P & S \\ \left( \begin{array}{ccc} 0 & -1 + A_1 \cos \omega t & 1 + A_2 \cos \omega t \\ 1 + A_3 \cos \omega t & 0 & -1 + A_4 \cos \omega t \\ -1 + A_5 \cos \omega t & 1 + A_6 \cos \omega t & 0 \end{array} \right) \end{array} \quad (7)$$

The three replicator equations (4) can be reduced to two equations on  $x_1$  and  $x_2$  by eliminating  $x_3$  via the constraint (2),  $x_3 = 1 - x_1 - x_2$ . The result is

$$\dot{x}_1 = x_1(1 - 2x_2 - x_1) + x_1 G_1(x_1, x_2; A_i) \cos \omega t \quad (8)$$

$$\dot{x}_2 = x_2(x_2 + 2x_1 - 1) + x_2 G_2(x_1, x_2; A_i) \cos \omega t \quad (9)$$

where  $G_1$  and  $G_2$  are polynomials in  $x_1$ ,  $x_2$  and the  $A_i$ 's (which we omit here for brevity). In the case that all the  $A_i$  coefficients are zero, equations (8) and (9) admit a first integral

$$x_1 x_2 (1 - x_1 - x_2) = \text{constant} \quad (10)$$

See Figure 1 where the integral curves (10) are displayed for various values of the constant. Each of these curves represents a motion which is periodic in

time. The points (1,0), (0,1), and (0,0), are equilibria for equations (8) and (9). The lines  $x_1=0$ ,  $x_2=0$  and  $x_1+x_2=1$ , are exact solutions for equations (8) and (9). Note that  $x_1+x_2=1$  is equivalent to  $x_3=0$  in view of equation (2). In the case that all the  $A_i$  coefficients are zero, there is another equilibrium at (1/3,1/3).

The presence of the time-varying periodic terms  $A_i \cos \omega t$  destroys the first integral (10). In addition, for general values of the  $A_i$  these terms destroy the equilibrium at (1/3), (1/3). We wish to consider the case in which this equilibrium is preserved under the periodic forcing. From equations (8) and (9), this will require that  $G_1$  and  $G_2$  vanish at  $x_1=x_2=1/3$ . This turns out to require the following relationship between the  $A_i$  coefficients

$$A_1 = A_6 + A_5 - A_2 \tag{11}$$

$$A_3 = A_6 + A_5 - A_4 \tag{12}$$

We choose the simple case  $A_1 = -A_2 = -A$ ,  $A_3 = A_4 = A_5 = A_6 = 0$ . This corresponds to the payoff matrix

$$\begin{matrix} & R & P & S \\ R & \begin{pmatrix} 0 & -1 - A \cos \omega t & 1 + A \cos \omega t \end{pmatrix} \\ P & \begin{pmatrix} 1 & 0 & -1 \end{pmatrix} \\ S & \begin{pmatrix} -1 & 1 & 0 \end{pmatrix} \end{matrix} \tag{13}$$

and to the following governing differential equations

$$\dot{x}_1 = x_1(1 - 2x_2 - x_1)[1 + (1 - x_1)A \cos \omega t] \tag{14}$$

$$\dot{x}_2 = x_2(x_2 + 2x_1 - 1 + [x_1(2x_2 + x_1 - 1)]A \cos \omega t) \tag{15}$$

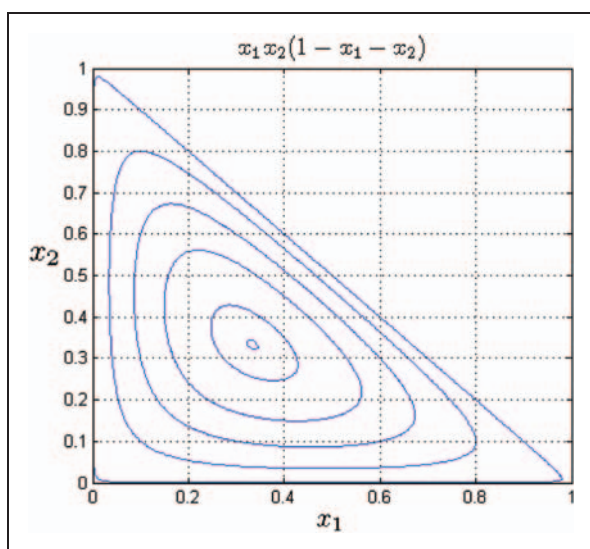


**Figure 1.** Integral curves from equation (10). Each of these curves represents a motion which is periodic in time.

Numerical integration shows that for small values of  $A$ , the periodic motions of the  $A=0$  system, given by equation (10), are typically replaced by quasiperiodic motions (Figure 2). In particular, motions starting near the equilibrium point (1/3,1/3) typically remain near it as in Figure 2. An exception occurs for certain values of the system parameters  $A$  and  $\omega$ . See Figure 3 which displays a numerically integrated motion starting near (1/3,1/3) for parameters  $A=0.1$ ,

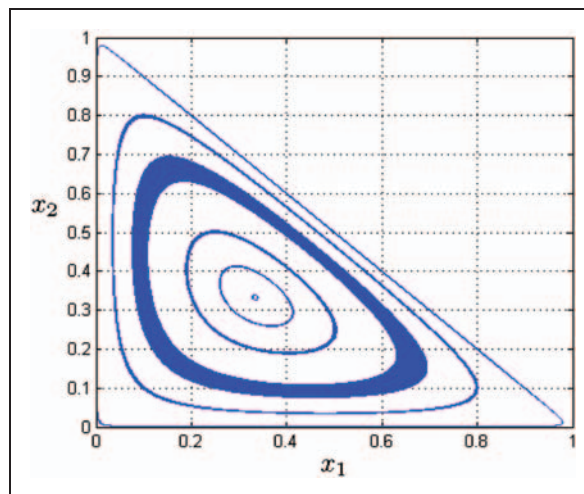


**Figure 2.** Motions of equations (14) and (15) for  $A=0.02$  and  $\omega=1$  obtained by numerical integration. Here, the periodic motions of Fig. 1 are replaced by quasiperiodic motions. Note that motions starting near the equilibrium point (1/3,1/3) remain near it.

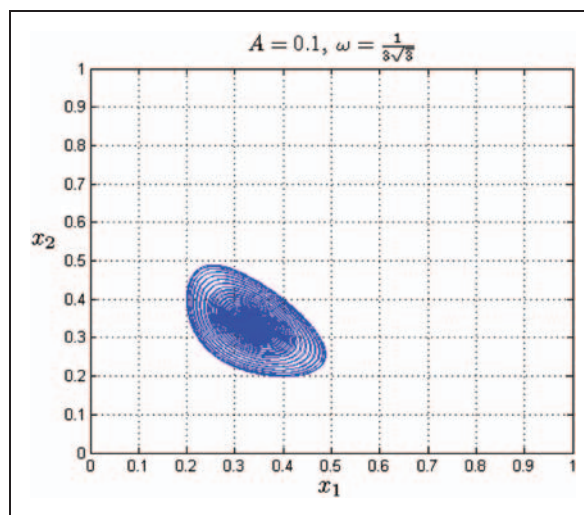


**Figure 3.** Motion of equations (14) and (15) for  $A=0.1$  and  $\omega=1.154$  for initial conditions  $x_1=x_2=0.333$  obtained by numerical integration. Note that here a motion which starts near the equilibrium (1/3,1/3) travels far away from it.

$\omega = 1.154$ . Note that here a motion which starts near the equilibrium  $(1/3, 1/3)$  travels far away from it.

In what follows we seek to explain this phenomenon using perturbation methods. In a previous work,<sup>10</sup> resonant values of the parameters  $\omega$  and  $A$  were identified using Floquet theory and associated instabilities of the equations linearized about the equilibrium point were studied. In this study, we investigate the behavior of the nonlinear equations of motion. This permits us to understand the structure of the phase space in the neighborhood of parametric resonances. That is, in the previous work we were able to predict which parameter values would lead to instabilities of the equilibrium point, whereas in this study we are able to build on the previous results and are able to say what happens away from the neighborhood of the equilibrium point, including bifurcations of periodic motions.

### Linear resonance

We begin by translating the origin to the equilibrium at  $(1/3, 1/3)$  and scaling the coordinates by  $\epsilon \ll 1$ . We set

$$x_1 = \epsilon x + \frac{1}{3}, \quad x_2 = \epsilon y + \frac{1}{3}, \quad (16)$$

and substitute these into equations (14) and (15), giving

$$\dot{x} = \frac{(3\epsilon x + 1)((3\epsilon x - 2)A \cos \omega t - 3)(2y + x)}{9} \quad (17)$$

$$\dot{y} = \frac{(3\epsilon y + 1)((6\epsilon x y + 2y + 3\epsilon x^2 + x)A \cos \omega t + 6x + 3y)}{9} \quad (18)$$

Our first step in the analysis of these ordinary differential equations (ODEs) is to determine which values of  $\omega$  produce instability via parametric resonance for small values of the forcing amplitude  $A$ . In the previous paper,<sup>10</sup> this was accomplished using Floquet theory. Here, we obtain this information directly from the perturbation method as follows. We first linearize (17) and (18) for small values of  $x$  and  $y$ . This can be done by setting  $\epsilon = 0$ , giving

$$\dot{x} = -\left(\frac{x + 2y}{3}\right) - \frac{2}{9}(2y + x)A \cos \omega t \quad (19)$$

$$\dot{y} = \left(\frac{2x + y}{3}\right) + \frac{1}{9}(2y + x)A \cos \omega t \quad (20)$$

Now, we look for a solution to these equations via regular perturbations, valid for small  $A \ll 1$ . The easiest way to do this is to transform this first-order system

of ODEs into a single second-order ODE by differentiating (19) and substituting expressions for  $\dot{y}$  from (20) and for  $y$  from (19), giving

$$f_1 \ddot{x} + f_2 \dot{x} + f_3 x = 0 \quad (21)$$

where

$$f_1 = 3 + 2A \cos \omega t \quad (22)$$

$$f_2 = 2A\omega \sin \omega t \quad (23)$$

$$f_3 = \left(\frac{3 + 2A \cos \omega t}{3}\right)^2 \quad (24)$$

We set

$$x = x_0 + A x_1 + O(A^2) \quad (25)$$

Substituting (25) into (21) and collecting terms gives

$$\ddot{x}_0 + \frac{x_0}{3} = 0 \quad (26)$$

$$\ddot{x}_1 + \frac{x_1}{3} = -\frac{2}{3}\ddot{x}_0 \cos \omega t - \frac{2}{3}\omega \dot{x}_0 \sin \omega t - \frac{4}{9}x_0 \cos \omega t \quad (27)$$

Equation (26) shows that  $x_0$  will have frequency  $1/\sqrt{3}$ , whereupon the right hand side of equation (27) will have terms with frequencies

$$\omega \pm \frac{1}{\sqrt{3}} \quad (28)$$

Resonant values of  $\omega$  will correspond to forcing frequencies (28) which are equal to natural frequencies of the homogeneous  $x_1$  equation, i.e. to  $1/\sqrt{3}$ . This gives that

$$\omega = \frac{2}{\sqrt{3}} \quad (\text{resonance}) \quad (29)$$

This value of  $\omega$  corresponds to the largest resonance tongue. There are an infinite of smaller tongues which would emerge from the perturbation method if we were to continue it to  $O(A^2)$  and higher. These have been shown<sup>10</sup> to be of the form  $\omega = 2/(n\sqrt{3})$  for  $n=2, 3, \dots$  but will not concern us in this study.

### Multiple scales perturbation method

The resonance (29) partially explains the phenomenon displayed in Figure 3: when  $\omega$  lies close to the resonant value of  $\frac{2}{\sqrt{3}}$ , motions which start near the equilibrium point ( $x=0, y=0$ ) (i.e.  $(x_1 = 1/3, x_2 = 1/3)$ ) may move relatively far away from it. This result is incomplete in

that it does not explain how far a motion will travel from the equilibrium point, or how the motion depends on initial conditions, or how close to the resonance value (29) the parameter  $\omega$  must be chosen for this phenomenon to occur. In this section of this article, we obtain approximate answers to these questions using a more powerful perturbation approach.<sup>13</sup>

We prepare for the perturbation expansion by setting  $\tau = \omega t$  and  $A = \epsilon^2$  in equations (17) and (18), and then again transforming the two first-order ODEs into a single second-order nonlinear ODE, giving

$$\begin{aligned}
 &18 \omega^2 (3 \epsilon x + 1) (3 \epsilon^3 x \cos \tau - 2 \epsilon^2 \cos \tau - 3) x'' = \\
 &81 \epsilon \omega^2 (6 \epsilon^3 x \cos \tau - 1) x'^2 \\
 &- 18 \epsilon^2 \omega^2 \sin \tau (3 \epsilon x - 2) (3 \epsilon x + 1) x' \\
 &- 243 \epsilon^9 x^6 \cos^2 \tau + 162 \epsilon^6 \cos \tau (2 \epsilon^2 \cos \tau + 3) x^5 \\
 &- 27 \epsilon^3 (\epsilon^4 \cos^2 \tau + 12 \epsilon^2 \cos \tau + 9) x^4 \\
 &- 18 \epsilon^4 \cos \tau (5 \epsilon^2 \cos \tau + 9) x^3 \\
 &+ 3 \epsilon (2 \epsilon^2 \cos \tau + 3) (2 \epsilon^2 \cos \tau + 9) x^2 \\
 &+ 2 (2 \epsilon^2 \cos \tau + 3)^2 x
 \end{aligned} \tag{30}$$

where primes represent differentiation with respect to  $\tau$ . Neglecting terms of  $O(\epsilon^3)$ , we obtain

$$\begin{aligned}
 \omega^2 x'' + \frac{x}{3} &= \frac{\epsilon(3\omega^2 x^2 - x^2)}{2} \\
 &- \frac{\epsilon^2(\omega^2(81xx'^2 + 12x'\sin\tau) - 27x^3 + 4x\cos\tau)}{18} \\
 &+ O(\epsilon^3)
 \end{aligned} \tag{31}$$

Next, we define three time scales  $\xi$ ,  $\eta$ , and  $\zeta$

$$\xi = \tau, \quad \eta = \epsilon \tau, \quad \zeta = \epsilon^2 \tau \tag{32}$$

and we consider  $x$  to be a function of  $\xi$ ,  $\eta$ , and  $\zeta$ , whereupon the chain rule gives

$$x' = x_\xi + \epsilon x_\eta + \epsilon^2 x_\zeta \tag{33}$$

$$x'' = x_{\xi\xi} + 2\epsilon x_{\xi\eta} + 2\epsilon^2 x_{\xi\zeta} + \epsilon^2 x_{\eta\eta} \tag{34}$$

We detune  $\omega$  off of the resonance (29)

$$\omega = \frac{2}{\sqrt{3}} + k\epsilon^2 + \dots \tag{35}$$

and expand  $x = x_0 + \epsilon x_1 + \epsilon^2 x_2 + \dots$ . Substituting (33) and (34) and these expansions into (31) and collecting terms, we obtain

$$Lx_0 = 0, \quad \text{where } L(\bullet) = (\bullet)_{\xi\xi} + \frac{1}{4}(\bullet) \tag{36}$$

$$Lx_1 = -\frac{3}{8}x_0^2 - 2x_{0\xi\eta} + \frac{3}{2}x_{0\xi}^2 \tag{37}$$

$$\begin{aligned}
 Lx_2 = &-\frac{3}{4}x_0x_1 + \frac{9}{8}x_0^3 - \sqrt{3}kx_{0\xi\xi} - \frac{1}{6}x_0 \cos \xi - 2x_{1\xi\eta} \\
 &- 2x_{0\xi\zeta} - x_{0\eta\eta} + 3x_{0\xi}x_{1\xi} - \frac{9}{2}x_0x_{0\xi}^2 - \frac{2}{3}x_{0\xi} \sin \xi \\
 &+ 3x_{0\eta}x_{0\xi}
 \end{aligned} \tag{38}$$

We take the solution of (36) in the form

$$x_0 = a_0(\eta, \zeta) \cos \frac{\xi}{2} + b_0(\eta, \zeta) \sin \frac{\xi}{2} \tag{39}$$

We substitute the expression for  $x_0$  (39) into the  $x_1$  equation (37), and remove secular terms, giving

$$\frac{\partial a_0}{\partial \eta} = 0, \quad \frac{\partial b_0}{\partial \eta} = 0 \quad \Rightarrow \quad a_0 = a_0(\zeta), \quad b_0 = b_0(\zeta) \tag{40}$$

Solving for  $x_1$ , we obtain

$$\begin{aligned}
 x_1 = &a_1(\eta, \zeta) \cos \frac{\xi}{2} + b_1(\eta, \zeta) \sin \frac{\xi}{2} + a_0 b_0 \sin \xi \\
 &- \frac{1}{2}b_0^2 \cos \xi + \frac{1}{2}a_0^2 \cos \xi
 \end{aligned} \tag{41}$$

Next, we substitute the expression for  $x_1$  (41) into the  $x_2$  equation (38), and remove secular terms, giving

$$\frac{\partial a_1}{\partial \eta} = f(a_0, b_0), \quad \frac{\partial b_1}{\partial \eta} = g(a_0, b_0) \tag{42}$$

where

$$f(a_0, b_0) = -\frac{da_0}{d\zeta} + \frac{b_0}{12} - \frac{\sqrt{3}}{4}kb_0 - \frac{3}{4}b_0^3 - \frac{3}{4}a_0^2b_0 \tag{43}$$

$$g(a_0, b_0) = -\frac{db_0}{d\zeta} + \frac{a_0}{12} + \frac{\sqrt{3}}{4}ka_0 + \frac{3}{4}a_0^3 + \frac{3}{4}b_0^2a_0 \tag{44}$$

Now, from equation (40), we see that  $a_0$  and  $b_0$  do not depend on  $\eta$ , which means that neither do  $f(a_0, b_0)$  or  $g(a_0, b_0)$ , and so equation (42) shows that  $a_1$  and  $b_1$  will grow linearly in time  $\eta$  unless  $f(a_0, b_0) = 0$  and  $g(a_0, b_0) = 0$ . Thus, for  $a_1$  and  $b_1$  to remain bounded, we require

$$\frac{da_0}{d\zeta} = \frac{b_0}{12} - \frac{\sqrt{3}}{4}kb_0 - \frac{3}{4}b_0^3 - \frac{3}{4}a_0^2b_0 \tag{45}$$

$$\frac{db_0}{d\zeta} = \frac{a_0}{12} + \frac{\sqrt{3}}{4}ka_0 + \frac{3}{4}a_0^3 + \frac{3}{4}b_0^2a_0 \tag{46}$$

This system of slow-flow equations is easier to deal with in polar coordinates

$$\frac{\partial r}{\partial \zeta} = \frac{1}{12} r \sin 2\theta, \quad \frac{\partial \theta}{\partial \zeta} = \frac{3}{4} r^2 + \frac{\cos 2\theta}{12} + \frac{\sqrt{3}}{4} k \quad (47)$$

where  $a_0 = r \cos \theta$  and  $b_0 = r \sin \theta$ .

In view of equation (39), equilibrium points in the slow-flow (47) correspond to periodic motions in the original system (14) and (15). The first of (47) gives  $\theta = 0, \pi/2, \pi, 3\pi/2$ , whereupon the second of (47) gives

$$\frac{3}{4} r^2 \pm \frac{1}{12} + \frac{\sqrt{3}}{4} k = 0 \Rightarrow r^2 = \mp \frac{1}{9} - \frac{\sqrt{3}}{3} k \quad (48)$$

Since  $r^2 > 0$ , we get bifurcations at

$$k = \pm \frac{1}{3\sqrt{3}} \quad (49)$$

For  $k > \frac{1}{3\sqrt{3}}$ , there are no nontrivial equilibria, while for  $k < -\frac{1}{3\sqrt{3}}$  there are four. In the intermediate case of  $-\frac{1}{3\sqrt{3}} < k < \frac{1}{3\sqrt{3}}$ , there are two nontrivial equilibria. From  $A = \epsilon^2$  and equation (35), the bifurcation curves have the form

$$\omega = \frac{2}{\sqrt{3}} \pm \frac{1}{3\sqrt{3}} A + \dots \quad (50)$$

which agrees with the location of stability transition curves in the study of Rand et al.<sup>10</sup> (Fig. 4).

The slow-flow (47) is conservative and admits the following first integral

$$9r^4 + 2(3\sqrt{3}k + \cos 2\theta)r^2 = \text{constant} \quad (51)$$

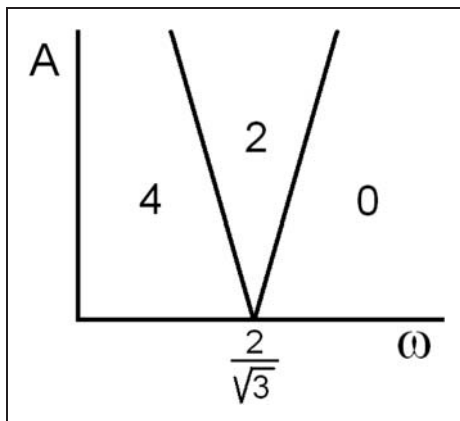


**Figure 4.** Bifurcation curves (50) showing the number of non-trivial equilibria in the slow flow (45) and (46). See Figure 5 for sample phase portraits of the slow flow in each of these regions.

Figure 5 displays the first integral (51) for  $k = \frac{1}{3\sqrt{3}} + 0.2 = 0.3925$ ,  $k = 0$ , and  $k = -\frac{1}{3\sqrt{3}} - 0.2 = -0.3925$ , respectively. Here, we have identified  $x$  with  $a_0$ , being approximately  $x_0$  at  $\xi = 0$  in equation (39). Similarly,  $x'$  is identified with  $b_0/2$ .

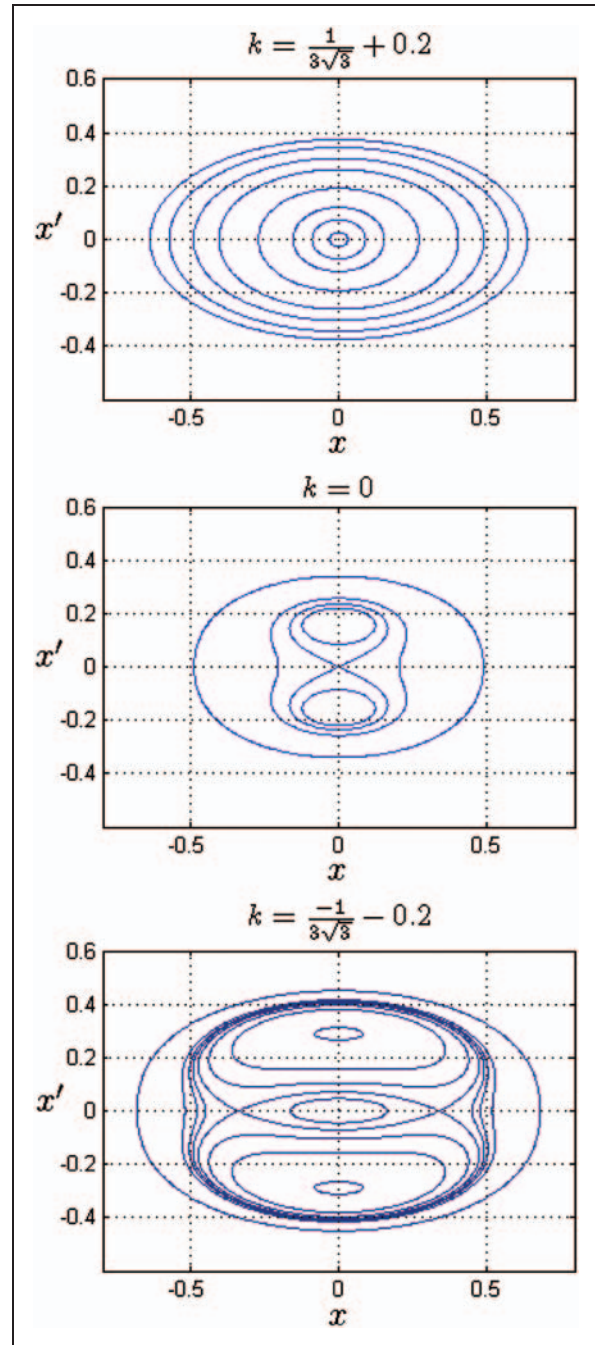


**Figure 5.** Plot of the first integral (51) for various values of  $k$ . Note, that as  $k$  decreases, the system traverses the tongue in Figure 4 from right to left and the number of nontrivial equilibria changes.

### Poincare map

The foregoing results of the perturbation method may be compared to numerical integration of equation (30) by use of a Poincare map. Here, we imagine a flow on a three-dimensional phase space with axes  $x, x', t$ , and an associated map produced by sampling the said flow at times  $\tau = 2N\pi$ , for  $N = 0, 1, 2, 3, \dots$ . The associated Poincare maps depend upon both  $\omega$  and  $\epsilon$ . Local behavior around the equilibrium point at the origin  $x = x' = 0$  is naturally affected by  $\omega$  as shown in Figure 5. The parameter  $\epsilon$  affects both the strength of the forcing (because the forcing amplitude  $A = \epsilon^2$ ) and the importance of nonlinearities (because the coordinates have been scaled by  $\epsilon$ , cf. equation (16)).

As a check on the perturbation results (which are expected to be valid for small  $\epsilon$ ), we first present Poincare maps for  $\epsilon = 0.1$  and for the same values of  $\omega$  as shown in Figure 5. See Figure 6. Note that there is good agreement in the neighborhood of the origin.

As an example of the kind of behavior which occurs for larger values of  $\epsilon$ , we present Poincare maps for  $\epsilon = 1$  and for the same values of  $k$  as shown in Figure 6. See Figure 7. These figures show the appearance of chaos which is associated with KAM theory.<sup>11</sup> KAM theory, named for its inventors, Kolmogorov, Arnold, and Moser, describes the onset of chaos in a perturbed Hamiltonian system. Among the various features of KAM theory is the phenomenon that chaos occurs most noticeably in the neighborhood of motions which in the unperturbed Hamiltonian system are in low-order resonance with the periodic driver. This is relevant to us here because equations (14) and (15) may be written in the form of a perturbed Hamiltonian system

$$\dot{x}_1 = \frac{\partial H}{\partial x_2} + \frac{A \cos \omega t}{h} \frac{\partial M}{\partial x_2} \tag{52}$$

$$\dot{x}_2 = -\frac{\partial H}{\partial x_1} - \frac{A \cos \omega t}{h} \frac{\partial M}{\partial x_1} \tag{53}$$

where

$$H = x_1 x_2 (1 - x_1 - x_2) \tag{54}$$

$$h = \frac{-1}{x_1(1 - x_1)^2(1 - x_1 - 2x_2)} \tag{55}$$

$$M = \frac{x_2}{x_1 - 1} \tag{56}$$

Thus, when  $A=0$ , the systems (14) and (15) are integrable and the Poincare map consists of closed curves as shown in Figure 1. Then, as predicted by KAM theory,

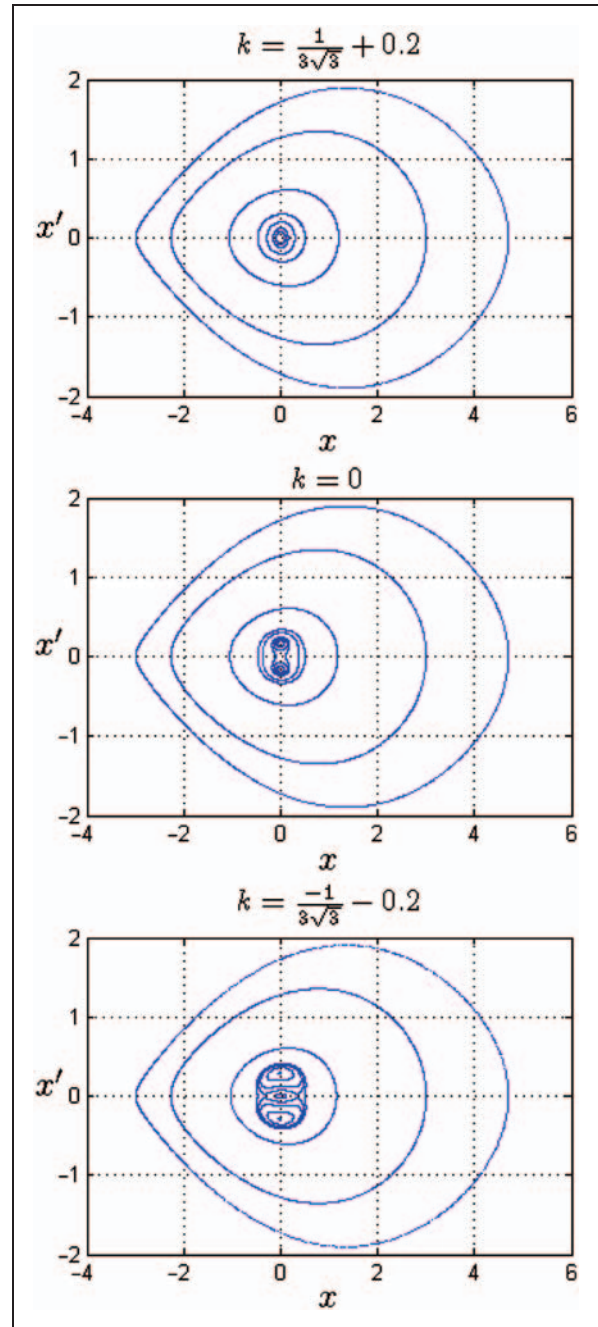


**Figure 6.** Poincare map obtained by numerically integrating equation (30) for  $\epsilon = 0.1$  and  $\omega = 2/\sqrt{3} + k\epsilon^2$ . Cf. Figure 5.

the closed curves in the Poincare map of the unperturbed Hamiltonian system which are in  $n : 1$  resonance with  $\cos \omega t$  are replaced by  $2n$ -cycles, one stable and one unstable. The stable  $n$ -cycle appears in simulations as  $n$  closed curves lying in the neighborhood of the unperturbed resonant curve. The unstable  $n$ -cycle appears as  $n$  saddles, each carrying a region of localized chaos with it. Some of these features may be seen in Figure 7.

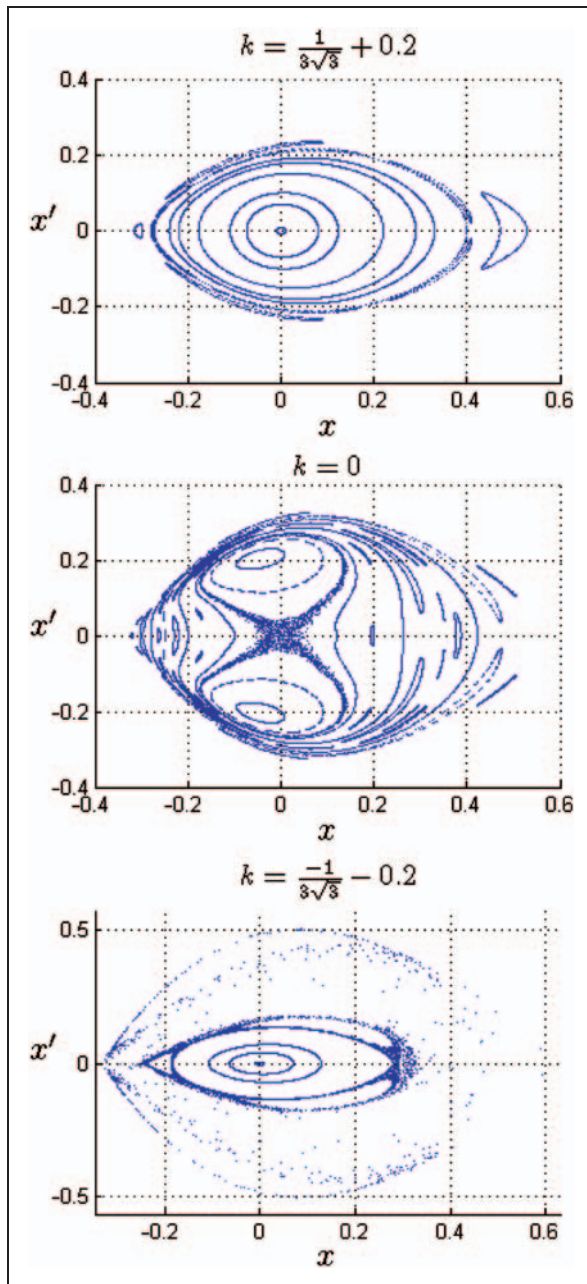


**Figure 7.** Poincaré map obtained by numerically integrating equation (30) for  $\epsilon = 1$  and  $\omega = 2/\sqrt{3} + k\epsilon^2$ . Cf. Figure 6.

## Conclusions

In this study, we have investigated the effect of adding periodic coefficients to a system which is more commonly treated as having constant coefficients. The system studied is a replicator equation based on an RPS scenario characterized by the payoff matrix (13) and governed by the differential equations (14) and (15). In the  $A=0$  constant coefficient case, this system is integrable with the first integral (10) and has the

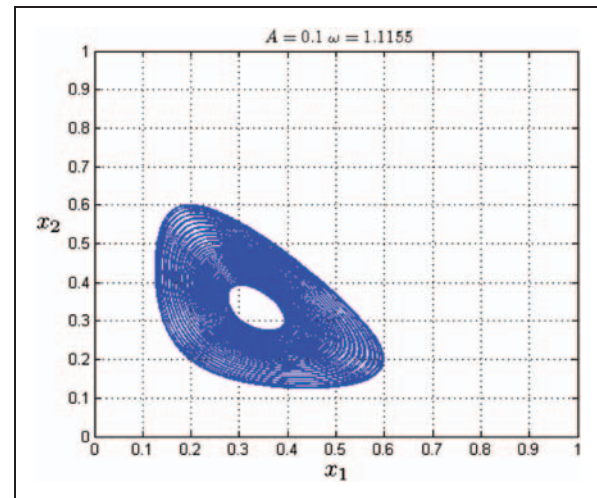


**Figure 8.** Motion of equations (14) and (15) for  $A=0.1$  and  $\omega = \frac{2}{\sqrt{3}} - (\frac{1}{3\sqrt{3}} + 0.2)A = 1.1155$  for initial conditions  $x_1 = x_2 = 0.3$  obtained by numerical integration. This system lies to the left of the resonance tongue in Figure 4. Note that here a motion which starts near the equilibrium  $(1/3, 1/3)$  travels far away from it.

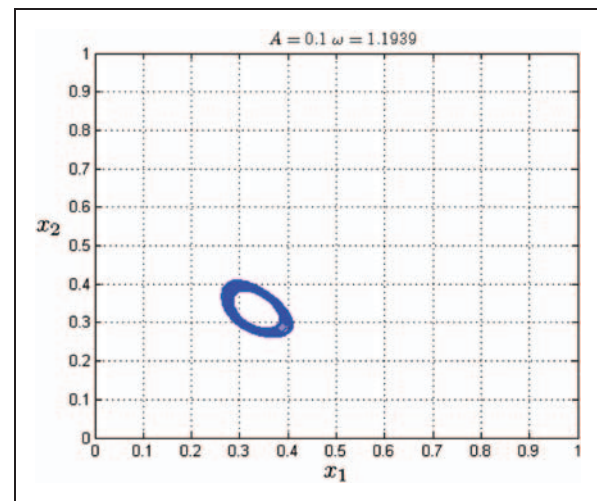


**Figure 9.** Motion of equations (14) and (15) for  $A=0.1$  and  $\omega = \frac{2}{\sqrt{3}} + (\frac{1}{3\sqrt{3}} + 0.2)A = 1.1939$  for initial conditions  $x_1 = x_2 = 0.3$  obtained by numerical integration. This system lies to the right of the resonance tongue in Figure 4. Note that here a motion which starts near the equilibrium  $(1/3, 1/3)$  remains close to it.

property that the equilibrium at  $(1/3, 1/3)$  is Liapunov stable (Figure 1). By contrast, in the  $A > 0$  system with periodic forcing, this same equilibrium can be unstable (Figure 3) due to parametric resonance (Figure 4). The analysis presented in this article, valid for small values of  $A$ , has shown that detuning off of this resonance is, however, unsymmetric. That is, systems which lie

outside and just to the left of the resonance tongue of Figure 4 have very different behavior from those systems which lie just to the right of the same tongue. (Figures 8 and 9). This behavior is predicted by the perturbation theory, cf. the Poincaré maps in Figure 5. For larger values of  $A$  we have seen that the system studied exhibits KAM type chaos (Figure 7).

Our results have implications for biological systems with RPS characteristics, such as the side-blotched lizard *Uta stansburiana* that displays persistent oscillations in population abundances.<sup>5</sup> Previous work has described the dynamics of this species using an evolutionary model with damping, and has attributed the persistence of the oscillations observed in the data to stochastic perturbations which reset the initial conditions (using a verbal rather than mathematical argument).<sup>5</sup> In this study, we have instead approached this issue by considering an external forcing function that drives the system via periodicity in the payoff coefficients. We showed how deterministic external forcing can lead to nonperiodic variation in population abundance.

### Funding

RER gratefully acknowledges financial support from the Sloan Foundation. DGR gratefully acknowledges financial support from the John Templeton Foundation's Foundational Questions in Evolutionary Biology Prize Fellowship.

### References

1. Nowak MA. *Evolutionary dynamics: exploring the equations of life*. Cambridge MA: Harvard Univ. Press, 2006.
2. Dreber A, Rand DG, Fudenberg D and Nowak MA. Winners don't punish. *Nature* 2008; 452: 348–351.
3. Rand DG, Ohtsuki H and Nowak MA. Direct reciprocity with costly punishment: generous tit-for-tat prevails. *J Theor Biol* 2009; 256: 45–57.
4. Schuster P and Sigmund K. Replicator dynamics. *J Theor Biol* 1983; 100: 533–538.
5. Sinervo B and Lively CM. The rockpapersissors game and the evolution of alternative male strategies. *Nature* 1996; 380: 240–243.
6. Kerr B, Riley MA, Feldman MW and Bohannan BJM. Local dispersal promotes biodiversity in a real-life game of rockpapersissors. *Nature* 2002; 418: 171–174.
7. Hauert C, De Monte S, Hofbauer J and Sigmund K. Volunteering as red queen mechanism for cooperation in public goods games. *Science* 2002; 296: 1129–1132.
8. Rand DG and Nowak MA. The evolution of anti-social punishment in optional public goods games. *Nat Commun* 2011; 2: 434.
9. Allahverdyan AE and Hu C-K. Replicators in a fine-grained environment: adaptation and polymorphism. *Phys Rev Let* 2009; 102: 058102.
10. Rand RH, Yazhbin M and Rand DG. Evolutionary dynamics of a system with periodic coefficients. *Commun Nonlinear Sci Numer Simulat* 2011; 16: 3887–3895.
11. Arnold VI and Avez A. *Ergodic problems of classical mechanics*. New York: Benjamin, 1968.
12. Hofbauer J and Sigmund K. *Evolutionary games and population dynamics*. Cambridge UK: Cambridge Univ. Press, 1998.
13. Rand RH. *Lecture Notes in Nonlinear Vibrations*, version 52. <http://www.math.cornell.edu/~rand/randdocs/nlvibe52.pdf> (2005). (accessed 1 September 2011).